Comparison of Diffusion Flux Models for Fischer-Tropsch Synthesis

Arvind. Nanduri[1] and Patrick L. Mills[*1]
[1]Texas A&M University-Kingsville, Department of Chemical & Natural Gas Engineering
*Corresponding author: Texas A&M University-Kingsville, Department of Chemical & Natural Gas Engineering, EC 303D, MSC 193, Kingsville, TX-78363-8202, USA. Email: Patrick.Mills@tamuk.edu

Abstract: The effect of various diffusion flux models (Wilke, Wilke-Bosanquet, Maxwell-Stefan, and Dusty Gas Model) on the Fischer-Tropsch (F-T) hydrocarbon product distribution was examined for diffusion and reaction in a 1-D isothermal spherical porous catalyst particle model. A Fe-based micro-kinetic olefin re-adsorption model developed by Wang *et al.* (2008) was coupled with the Soave-Redlich-Kwong (SRK) equation of state to describe the particle-scale transport-kinetic interactions and phase behavior for the gas-phase Fischer-Tropsch Synthesis (FTS) [3]. The role of the catalyst mean pore diameter on the FT product distribution was also studied when both Knudsen and molecular diffusion are included. The intra-particle concentration profiles of key reactants and diesel range hydrocarbons, liquid-to-vapor ratio, CO conversion and intra-particle methane-based diesel selectivity were also determined for each multi-component flux models to assess their effect on particle-scale performance.

Keywords: Multi-component diffusion flux models, Fischer-Tropsch Synthesis, vapor-liquid-equilibrium (VLE), gas phase micro-kinetics.

1. Introduction

The Fischer-Tropsch Synthesis (FTS) is a highly exothermic polymerization reaction of syngas ($CO+H_2$) in the presence of Fe/Co/Ru-based catalysts to produce a wide range of paraffins, olefins and oxygenates, which is often called *syncrude*. Multi-Tubular Fixed Bed Reactors (MTFBR) and Slurry Bubble Column reactors (SBCR) are widely employed for FTS processes [1]. To understand the reactor-scale catalyst performance, it is important to first study the particle-scale transport-kinetic interactions.

Since the FTS is a polymerization reaction that can produce hydrocarbons with carbon numbers ranging from 1 to 100, the catalyst pores in this process can be filled with liquid wax (C_{20}+) leading to high diffusional limitations. To comprehensively model such a reaction network, micro-kinetic rate expressions for each individual species must be coupled with the intraparticle solubility of gases in the liquid wax and transport equations for the various reaction species in the porous catalyst. Temperature-based correlations for diffusivities of F-T products in wax are widely used, although a comparison of diffusion flux models (Wilke, Wilke-Bosanquet, Maxwell-Stefan, and Dusty Gas Model) to describe species transport-kinetic interactions for FTS has not been reported in the open literature [2]. In this paper, the aforementioned multi-component diffusion flux models for FTS are incorporated into a transport-kinetics model for a spherical porous catalyst shape and compared using COMSOl Multiphysics™ as the numerical modeling platform analysis.

2. Catalyst Pellet Model

The isothermal 1-D catalyst pellet model used to describe transport-kinetic interactions is presented in this section.

A total number of 20 paraffins (C_1 to C_{20}), 19 olefins (C_2 to C_{20}) and 4 key reaction components (H_2, CO, CO_2, and H_2O) are considered in the reaction network, which leads to 43 nonlinear differential equations for the specie mass balances. The micro-kinetic and thermodynamic expressions used in the model can be found elsewhere [2-4].

2.1 Specie mass balance equations and diffusion flux models

The specie mass balance equation for a spherical pellet is given below in which the parameter $\xi = r/R_P$ is the dimensionless radius.

$$\frac{1}{\xi^2}\frac{\partial}{\partial \xi}\left(D_{ei}\xi^2\frac{\partial C_i}{\partial \xi}\right) = -\rho_p R_p{}^2 \sum_j \alpha_{ij} R_{ij}$$

$$\xi = \frac{r}{R_p}$$

The temperature-based F-T specie diffusivity correlations and the multi-component molar diffusion fluxes used here are described according to Wilke, Wilke-Bosanquet, Maxwell-Stefan and Dusty Gas models. The working equations are summarized below.

Wang Diffusion Flux Model [2]

$$N_i = -D_{ei}\nabla C_i$$

$$D_{ei} = \frac{\varepsilon D_{i,B}}{\tau} \qquad D_{i,B} = D_{CO,B}\left(\frac{V_{CO}}{V_i}\right)^{0.6}$$

$$D_{CO,B} = 5.584 * 10^{-7} e^{-\frac{1786.29}{T}}$$

$$D_{H_2,B} = 1.085 * 10^{-6} e^{-\frac{1624.63}{T}}$$

$$D_{CO_2,B} = 3.449 * 10^{-7} e^{-\frac{1613.65}{T}}$$

Wilke Model

$$N_i = -D_{im}\nabla C_i$$

$$D_{im} = \frac{1 - x_i}{\sum_{j=1,j\neq i}^{n} \frac{x_j}{\widetilde{D_{ij}}}}$$

$$\widetilde{D_{ij}} = \frac{0.00266\, T^{\frac{3}{2}}}{P M_{ij}^{\frac{1}{2}} \sigma_{ij}^{2} \Omega_{D,ij}}$$

Wilke-Bosanquet Model

$$N_i = -D_{i,eff}\nabla C_i$$

$$\frac{1}{D_{i,eff}} = \frac{1}{D_{im}} + \frac{1}{D_{ik}}$$

$$D_{ik} = \frac{2\varepsilon a}{3\tau}\sqrt{\frac{8RT}{\pi M_i}}$$

Maxwell-Stefan Model

$$N_i = \frac{-\nabla C_i + \sum_{j=1,j\neq i}^{n} \frac{x_i N_j}{\widetilde{D_{ij}}}}{\sum_{j=1,j\neq i}^{n} \frac{x_j}{\widetilde{D_{ij}}}}$$

Dusty Gas Model (DGM)

$$N_i = \frac{-\nabla C_i + \sum_{j=1,j\neq i}^{n} \frac{x_i N_j}{\widetilde{D_{ij}}}}{\sum_{j=1,j\neq i}^{n} \frac{x_j}{\widetilde{D_{ij}}} + \frac{1}{D_{ik}}}$$

2.2 Boundary conditions

The boundary conditions correspond to specified concentrations at the pellet surface, which correspond to Dirichlet conditions.

At $\xi = -1$ and $\xi = 1$, $C_i = C_{i,bulk}$

2.3 Vapor-Liquid-Equilibrium calculations

The vapor-liquid equilibrium for the FTS reaction mixture is described by the Soave-Redlich- Kwong equation of state [3]. The flash calculations are based upon satisfying the Rachford-Rice objective function:

$$F(\alpha_g) = \sum_i \frac{z_i(K_i - 1)}{\left(1 + \alpha_g(K_i - 1)\right)} = 0$$

In this application, the Rachford-Rice objective function is a polynomial of degree 43 (43 distinct roots). Since the fraction $\alpha_g = V/(V+L)$ is a positive number < 1, only the roots that make physical sense are considered. The initial estimate of the distribution coefficient is obtained from Wilson's correlation [3]:

$$K_i^{\text{guess value}} = \frac{P_{ic}}{P}\exp\left(5.37(1+\omega_i)\left(1 - \frac{T_{ic}}{T}\right)\right)$$

Here, the distribution coefficient is defined as the ratio of the vapor to liquid mixture fugacity coefficients:

$$K_i = \frac{\emptyset_i^{V}}{\emptyset_i^{L}}$$

3. Use of COMSOL Multiphysics

The 1-D diffusion-reaction system was solved using the *Transport of Diluted Species* module in COMSOL Multiphysics™ assuming steady-state conditions. The Rachford-Rice objective function (VLE calculations) was solved

using the coefficient form of the PDE solver. The catalyst properties and operating conditions used in the models are listed in Tables 1 - 2. The solution for the specie concentration profiles were based upon a convergence factor of 10^{-3}.

To avoid convergence issues, the particle radius was set to a small number (0.01 mm) and the subsequent solution was used as initial conditions for larger values of the particle radius until the target radius of R_p = 1.5 mm was reached. The numerical instabilities and the use of inbuilt logical operators to avoid negative specie concentrations are discussed elsewhere [6]. Mesh refinement was manually performed until the concentration profiles were relatively constant and satisfied the convergence criterion.

Table 1. Catalyst properties

Density of pellet, ρ_p	1.95 x 10^6 (gm/m^3)
Porosity of pellet,ε	0.51
Tortuosity, τ	2.6
Sphere radius, R_p	1.5 mm

Table 2. Operating conditions.

Temperature, ^oK	493
Pressure, bar	25
H_2/CO	2

4. Results

4.1 Concentration profiles of key reactants

The 1-D isothermal concentration profiles of the key components (H_2, CO, CO_2 and H_2O) under typical FTS operating conditions for different multi-component flux models are shown in Figure 1 - 4. The Dusty Gas and Wilke-Bosanquet models account for both Knudsen and molecular diffusion. The mean catalyst pore diameter of a typical Fe-based FT catalyst is about 25 nm. The role of the mean pore diameter on F-T product distribution is discussed in Section 4.3. The profiles show that the CO concentration approaches zero for the Dusty Gas (DGM), and Wang models (temperature-based diffusivity correlations), but the Wilke and Maxwell-Stefan flux models predict low conversion of CO in the F-T reaction network. The CO_2 concentration reaches a peak and then decreases due to the reverse Water-Gas-Shift (WGS) reaction. The reverse WGS reaction produces CO, which is then consumed in the subsequent hydrocarbon-producing F-T reactions. The reverse WGS reaction is predicted by the DGM and Wang model whereas the Wilke, Wilke-Bosanquet and Maxwell-Stefan models *do not* predict the reverse WGS reaction.

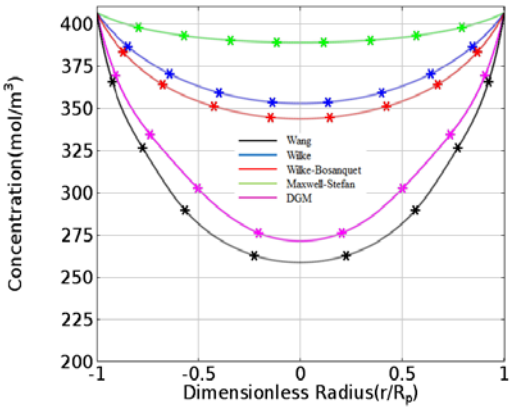

Figure 1. Concentration profile of H_2 in a spherical catalyst pellet (radius R_p = 1.5 mm, mean pore diameter a = 25 nm, T = 493 K, P = 25 bar, and H_2/CO = 2).

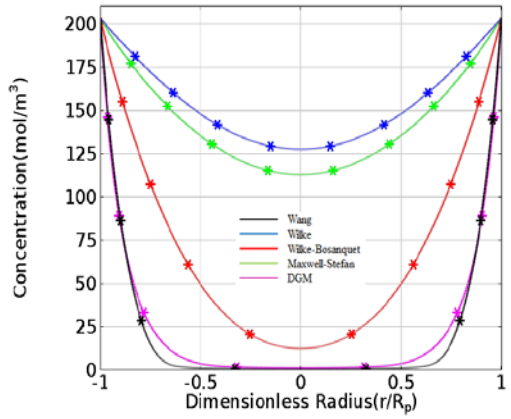

Figure 2. Concentration profile of CO in a spherical catalyst pellet (radius R_p = 1.5 mm, mean pore diameter a = 25 nm, T = 493 K, P = 25 bar, and H_2/CO = 2).

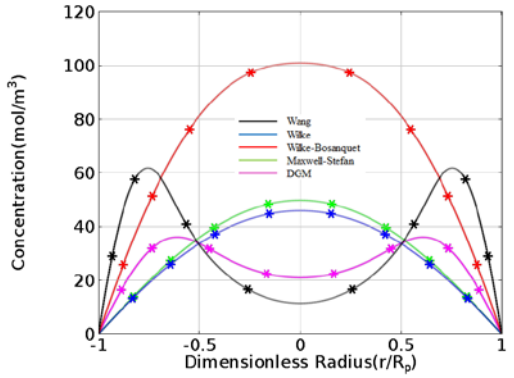

Figure 3. Concentration profile of CO_2 in a spherical catalyst pellet (radius R_p = 1.5 mm, mean pore diameter a = 25 nm, T = 493 K, P = 25 bar, and H_2/CO = 2).

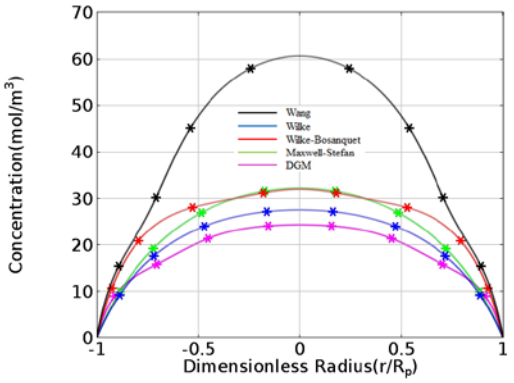

Figure 4. Concentration profile of H_2O in a spherical catalyst pellet (radius R_p = 1.5 mm, mean pore diameter a = 25 nm, T = 493 K, P = 25 bar, and H_2/CO = 2).

4.2 Intra-particle liquid-to-vapor ratio

The intra-particle liquid-to-vapor molar ratio (L/V) for different flux models is shown in Figure 5. These results show that the temperature-based flux model (Wang Model) predicts a high L/V ratio when compared to Wilke, Wilke-Bosanquet, Maxwell-Stefan and DGM models. This result is also supported by comparing concentration profiles of key components (see Figures 1 - 4) where the CO concentration rapidly approaches to zero in Wang model due to significant diffusional limitation in liquid wax. The Wilke-Bosanquet and DGM models also predict a similar trend for the CO concentration, but the diffusional limitation in these models corresponds to Knudsen diffusion in the catalyst pores. These results also show the importance of understanding the phase behavior of FT products in the catalyst pores since the reaction kinetics for liquid phase and gas phase would differ.

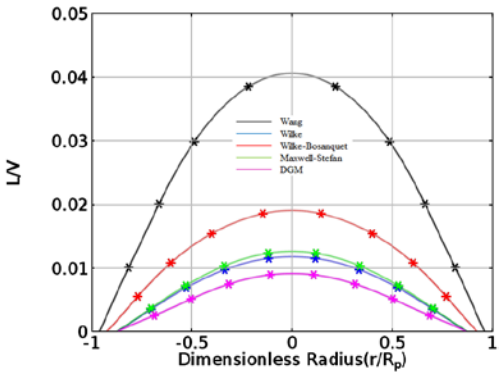

Figure 5. Intra-particle liquid-to-vapor ratio for a spherical catalyst pellet (radius R_p = 1.5 mm, mean pore diameter a = 25 nm, T = 493 K, P = 25 bar, and H_2/CO = 2).

4.3 Intra-particle methane-based diesel selectivity and concentration profiles in the diesel range

The concentration profiles of the diesel range and the intra-particle methane-based diesel selectivity ($S_{i,CH4}$) for the multicomponent flux models are shown in Figures 6 - 7. The Wang model predicts a high concentration in the diesel range due to the reverse WGS reaction producing CO, which is then consumed in the subsequent hydrocarbon producing F-T reactions. The DGM predicts the lowest concentration of diesel range. This can be due to the strong influence of Knudsen diffusion on the F-T reaction chemistry.

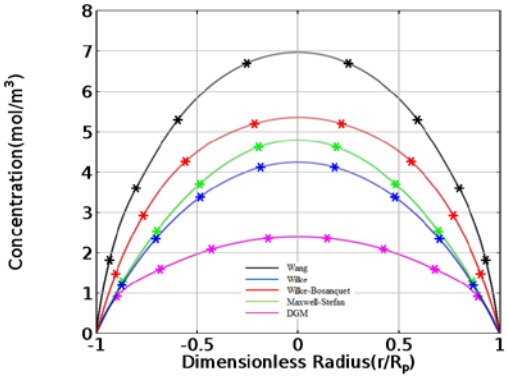

Figure 6. Concentration profile in the diesel range in a spherical catalyst pellet (radius R_p = 1.5 mm, mean

pore diameter a = 25 nm, T = 493 K, P = 25 bar, and $H_2/CO = 2$).

The magnitude of the decrease in the methane-based diesel selectivity ($S_{i,CH4}$) is higher in the case of the temperature-based diffusivity correlations (Wang), DGM and Wilke-Bosanquet when compared to Wilke and Maxwell-Stefan models. This occurs because the Wilke and Maxwell-Stefan models do not account for the collision of gas molecules with the pore walls, leading to inaccurate predictions of specie concentrations [7]. It can also be noted from the multi-component flux equations (summarized in section 2.1), that only the Wilke-Bosanquet and DGM models account for collision of molecules with the catalyst pore walls by including the Knudsen diffusion coefficient term. It is also observed that the methane-based diesel selectivity starts to increase for both the Wang and DGM models due to the reverse WGS reaction and also the olefin re-adsorption, which results in an increase in diesel concentration. The specie concentration and product distribution in a porous catalyst is often dictated by the magnitude of catalyst mean pore diameter. These results show the importance of understanding the coupled effect of Knudsen and continuum/molecular diffusion to study the dynamics of a multi-component reaction-diffusion system, like F-T synthesis, in a porous catalyst.

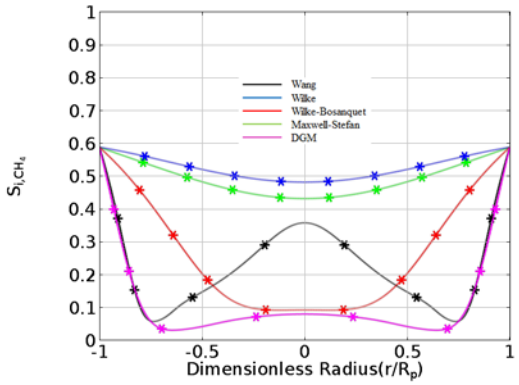

Figure 7. Intra-particle methane-based diesel selectivity in a spherical catalyst pellet (radius R_p = 1.5 mm, mean pore diameter a = 25 nm, T = 493 K, P = 25 bar, and $H_2/CO = 2$).

4.4 Effect of catalyst mean pore diameter

As discussed in the previous section, it is imperative to study the effect of catalyst mean pore diameter on the specie concentration profiles. The effect of pore diameter, through Knudsen diffusion, on the intra-particle CO_2 concentration profiles, methane-based diesel selectivity and intra-particle liquid-to-vapor ratio will be discussed in this section. The key results are shown in Figure 8 - 13.

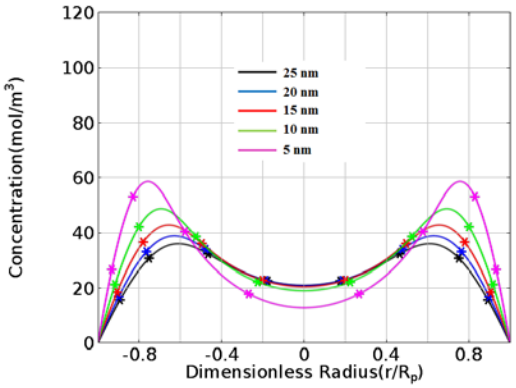

Figure 8. Intra-particle CO_2 concentration profiles for DGM in a spherical catalyst pellet (radius R_p = 1.5 mm, mean pore diameter a = **25 nm**, **20 nm**, **15 nm**, **10 nm** & **5 nm**, T = 493 K, P = 25 bar, and $H_2/CO = 2$).

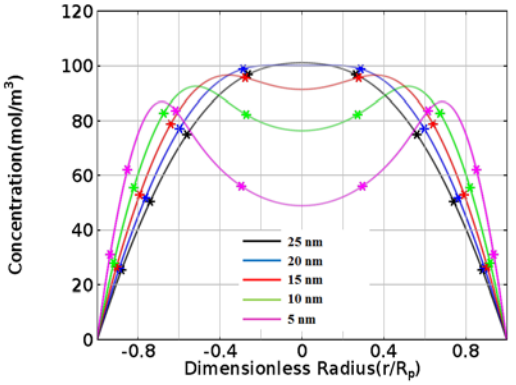

Figure 9. Intra-particle CO_2 concentration profiles for Wilke-Bosanquet model in a spherical catalyst pellet (radius R_p = 1.5 mm, mean pore diameter a = **25 nm**, **20 nm**, **15 nm**, **10 nm** & **5 nm**, T = 493 K, P = 25 bar, and $H_2/CO = 2$).

It can be observed in Figure 8 and 9 that the reverse WGS reaction becomes significant with decreasing pore diameter values for both the DGM and Wilke-Bosanquet models. The reverse WGS is observed only for the mean pore diameter values of less than 20 nm whereas the DGM predicts the reverse WGS for all the mean pore diameter values considered in this work (25 nm, 20 nm, 15 nm, 10 nm & 5 nm). This can be

explained by noting that for the Wilke-Bosanquet model, the contribution of molecular diffusion is defined on the basis of the Wilke model, which does not account for strong molecular interactions [7, 8], and the Knudsen diffusion is not significant for large pore diameter values. In the case of the DGM, the molecular diffusion term is similar to Maxwell-Stefan model, which accounts for significant molecular interactions [8]. The strong coupling between the Knudsen and continuum diffusion terms in DGM is responsible for the reverse WGS reaction in all the pore diameters considered in this study.

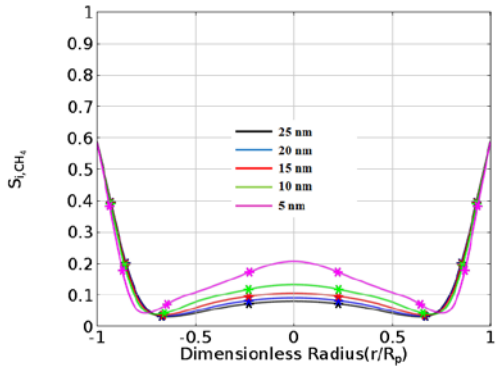

Figure 10. Intra-particle methane-based diesel selectivity for DGM in a spherical catalyst pellet (radius R_p = 1.5 mm, mean pore diameter a = **25 nm**, **20 nm**, **15 nm**, **10 nm** & **5 nm**, T = 493 K, P = 25 bar, and H_2/CO = 2).

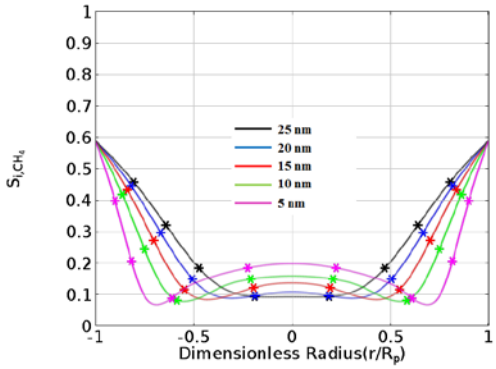

Figure 11. Intra-particle methane-based diesel selectivity for Wilke-Bosanquet model in a spherical catalyst pellet (radius R_p = 1.5 mm, mean pore diameter a = **25 nm**, **20 nm**, **15 nm**, **10 nm** & **5 nm**, T = 493 K, P = 25 bar, and H_2/CO = 2).

The intra-particle methane-based diesel selectivity (Figure 10 & 11) follows an exact opposite trend with the increase in catalyst mean pore diameter as compared to the CO_2 concentration profile for both DGM and Maxwell-Stefan models. As discussed in section 4.3, the increase in the rate of reverse WGS reaction and also significant olefin re-adsorption in small pore diameters results in an increase in diesel range hydrocarbon concentration. This leads to higher diesel selectivity when compared to that obtained using large pore diameters.

The increasing trend in the intra-particle liquid-to-vapor ratio for both DGM and Wilke-Bosanquet models with decreasing pore diameters is not surprising since the long-chain hydrocarbons would be present in the F-T wax in catalyst pores with small diameters. These results show that the information about catalyst pore size distribution is crucial to understand the diffusional limitations encountered by the F-T reactants in the presence of liquid wax.

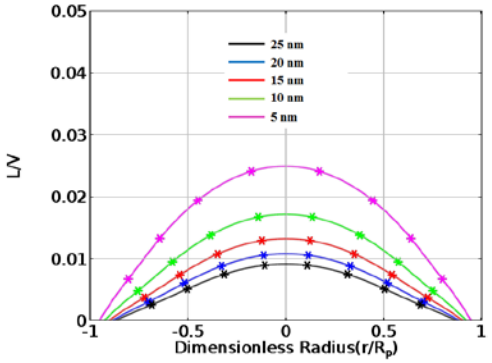

Figure 12. Intra-particle liquid-to-vapor ratio for DGM in a spherical catalyst pellet (radius R_p = 1.5 mm, and mean pore diameter a = 25 nm, 20 nm, 15 nm, 10 nm & 5 nm).

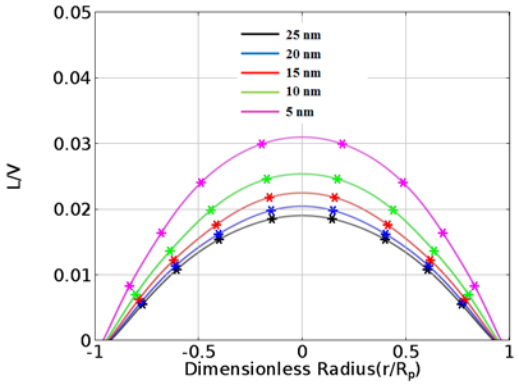

Figure 13. Intra-particle liquid-to-vapor ratio for Wilke-Bosanquet model in a spherical catalyst pellet (radius R_p = 1.5 mm, and mean pore diameter a = 25 nm, 20 nm, 15 nm, 10 nm & 5 nm).

5. Conclusions

The effect of various multicomponent flux models (Wilke, Wilke-Bosanquet, Maxwell-Stefan, and Dusty Gas models) on the transport-kinetic interactions for FTS in a 1-D catalyst pellet model using a detailed micro-kinetic model was successfully analyzed for the first time using COMSOL Multiphysics™. The temperature-based diffusivity correlations do not take into consideration the change in the effective diffusivities of species in a reaction-diffusion system. This work demonstrates that COMSOL can be a powerful numerical engine in solving complex multicomponent diffusion flux models. I t is also shown that catalyst properties, such as pore size distribution, can play a major role in understanding the intra-particle FT product distribution. The inclusion of Knudsen diffusion in the Wilke-Bosanquet and DGM models produce results that closely approximate the FT product distribution of the Wang model due to the formation of CO through reverse WGS reaction which, in-turn, participates in the FT reaction network producing hydrocarbons. The results in the current work will provide the basis to compare the flux models on a reactor-scale and analyze the FT product distribution and diesel selectivity in a packed bed reactor.

6. Nomenclature

a	Average pore diameter (nm)
C_i	Concentration of species 'i' (mol/m^3)
$C_{i,bulk}$	Concentration of species 'i' in bulk phase (mol/m^3)
D_{ei}	Effective diffusivity of species 'i' (m^2/s)
$D_{i,B}$	Bulk diffusivity of component i (m^2/s)
D_{im}	Multi-component diffusivity of component i (m^2/s)
$\widetilde{D_{ij}}$	Binary diffusion coefficient (cm^2/s)
D_{ik}	Knudsen diffusion coefficient (m^2/s)
K_i	Equilibrium ratio
L	Number of moles in the liquid phase (moles)
M_i	Molecular weight of component i (gm/g mole)
N_i	Specie molar flux (mol m^{-2} s^{-1})
P	Pressure (bar)
P_{ic}	Critical pressure of component i (bar)
r	Radial coordinate (mm)
R_p	Radius of catalyst pellet (mm)
R_{ij}	Rate of component i in jth reaction (mol kg^{-1} s^{-1})
$S_{i,CH4}$	Methane-based diesel selectivity $\left(\frac{\Sigma_{i,j}\alpha_{ij}R_{ij}}{\Sigma_{CH_4,j}\alpha_{CH_4,j}R_{CH_4,j}}\right)$
T	Temperature (K)
T_{ic}	Critical temperature of component i (K)
V	Number of moles in vapor phase
V_{CO}	Molar volume of CO (m^3/mol)
V_i	Molar volume of component i (m^3/mol)
z_i	Number of moles of component i
Greek Letters	
α_g	Intra-particle vapor fraction
α_{ij}	Stoichiometric coefficient of component i in reaction j
ξ	Radial coordinate, dimensionless
ρ_p	Density of catalyst pellet (kg/m^3)
ε	Catalyst pellet porosity
τ	Catalyst tortuosity

7. References

1. D. A. Wood, C. Nwaoha, and B. F. Towler, Gas-To-Liquids (GTL): A Review of an Industry Offering Several Routes for Monetizing Natural Gas, *Journal of Natural Gas Science and Engineering*, **9**, 196-208 (2012).
2. Yi-Ning Wang, Yuan-Yuan Xu, Hong-Wei Xiang, Yong-Wang Li, and Bi-Jiang Zhang, Modeling of Catalyst Pellets for Fischer-Tropsch Synthesis, *Industrial & Engineering Chemistry Research*, **40**, 4324-4335 (2001).
3. Y. N. Wang, Y. W. Li, L. Bai, Y. L. Zhao, and B. J. Zhang, Correlation for Gas-Liquid Equilibrium Prediction in Fischer-Tropsch Synthesis, *Fuel*, **78**, 911-917 (1999).
4. Yi-Ning Wang, Wen-Ping Ma, Yi-Jun Lu, Jun Yang, Yuan-Yuan Xu, Hong-Wei Xiang, Yong-Wang Li, Yu-Long Zhao, Bi-Jiang Zhang, Kinetic Modelling of Fischer-Tropsch Synthesis Over an Industrial Fe-Cu-K Catalyst, *Fuel*, **82**, 195-213 (2003).
5. Yong Yang, Hong-Wei Xiang, Yuan-Yuan Xu, Liang Bai, Yong-Wang Li, Effect of Potassium Promoter on Precipitated Iron-Manganese Catalyst for Fischer-Tropsch Synthesis, *Applied Catalysis A: General*, **266**, 181-194 (2004).
6. Arvind Nanduri, and Patrick L. Mills, Diffusion and Reaction in Fe-Based Catalyst for Fischer-Tropsch Synthesis Using Micro Kinetic Rate Expressions, *Proceedings of the 2014 COMSOL Conference in Boston* (2014).
7. Stephen W. Webb, and Karsten Pruess, The Use of Fick's Law for Modeling Trace Gas Diffusion in Porous Media, *Transport in Porous Media*, **51**, 327-341 (2003).
8. R. Krishna, and J. A. Wesselingh, The Maxwell-Stefan Approach to Mass Transfer, *Chemical Engineering Science*, **52**, 861-911 (1997).